Hindawi
Shock and Vibration
Volume 2023, Article ID 4578613, 11 pages
https://doi.org/10.1155/2023/4578613

Research Article

Development of an Impact Energy Absorption Structure by an Arc Shape Stroke Origami Type Hydraulic Damper

Jingchao Guan,[1] **Yuan Yao**,[1] **Wei Zhao**,[2] **Ichiro Hagiwara**,[3] **and Xilu Zhao**[1]

[1]*Department of Mechanical Engineering, Graduate School, Saitama Institute of Technology, Saitama 369-0293, Japan*
[2]*National Institute of Technology, Toyama College, Toyama 939-8630, Japan*
[3]*Organization for the Strategic Coordination of Research and Intellectual Property, Meiji University, Tokyo 101-8301, Japan*

Correspondence should be addressed to Jingchao Guan; guanjingchao123@gmail.com

Received 21 August 2023; Revised 20 November 2023; Accepted 30 November 2023; Published 9 December 2023

Academic Editor: Fehmi Najar

Cylindrical hydraulic dampers used to reduce impacts and vibrations typically have linear strokes. In this study, a new arc-shaped stroke-type origami hydraulic damper with a nonlinear damping performance was proposed. By examining the damping effect of the origami hydraulic damper, the damping force was found to be proportional to the square of the motion velocity. A nonlinear dynamics governing equation was established using the derived formula for the damping force of the origami hydraulic damper, and a numerical analysis using the Runge–Kutta method was established. An impact test device with an arc-shaped stroke was developed, and the error between the numerical analysis value of the impact displacement and the measured experimental value was confirmed to be sufficiently small. An impact verification experiment confirmed that the damping effect of the origami hydraulic damper increases with the input energy of the impact. By varying the diameter of the orifice hole, which is an important design factor for an origami hydraulic damper, the damping effect of the origami hydraulic damper was found to increase as the diameter of the orifice hole decreased. To examine the effect of the type of hydraulic oil inside the origami hydraulic damper, water and edible oil were used to conduct impact verification experiments, and it was found that the effect on the impact damping effect was relatively small.

1. Introduction

Cylinder-type hydraulic dampers are widely used as energy-absorbing parts for impact- and vibration-damping devices, and several research results on their damping performance against impact vibrations and the development of applied technology have been published [1–6].

Hydraulic dampers are employed to effectively absorb the energy of automobiles, impacting complex road vibrations and obstacles, with the aim of improving passenger comfort and safety as much as possible [7–11]. In high-speed trains running at higher than normal speeds, problems such as changes in the damping characteristics of hydraulic dampers and instability with increasing running speed have been studied [12, 13]. In the construction industry, the effectiveness of installing semiactive hydraulic dampers along the diagonal direction of the rectangular frame of a main structure has been verified to reduce the damage to buildings and bridges caused by earthquakes [14–16]. In addition, magnetorheological (MR) dampers, which use a magnetic field, have been developed to improve the performance of cylinder-type hydraulic dampers, and several research results have been published [17–22].

However, the current hydraulic damper is a cylindrical type that can only move in one direction, and the length that can be expanded, contracted, and used as a hydraulic damper is limited. Therefore, it is difficult to use when the installation space is limited. In addition, when the goal of weight reduction is pursued, it is desirable that the cylinder damper be constructed with a simpler shape and lighter materials than metal cylinder dampers. Furthermore, considering three-dimensional complex usage conditions, if there is not only a dynamic load along the axial direction but also a random load along the lateral direction, problems

such as wear of the cylinder seal and stress concentration can occur. Therefore, instead of metal cylinder-type hydraulic dampers, research and development of a new lightweight nonmetallic hydraulic damper that can flexibly cope with three-dimensional random load conditions are required.

In recent years, origami structures, which have been proposed to satisfy the requirements of a wide range of industrial fields, have been studied from the basic viewpoints of geometry and mechanics [23–27]. Among these, the tubular origami structure, which can be freely folded along the axial direction, has the potential to be applied instead of the conventional metal cylinder-type damper. The geometry of such foldable tubular origami structures and their deformation properties under external forces have been investigated [28–36]. Light weight and flexibility are required for robotic arms in the research and development of automatic control. Taking advantage of the characteristics of foldable tubular origami structures, studies are underway to apply them to robot arms, hands, and grippers [37–39]. In addition, by applying an external force to the inside or partial structure of a foldable tubular origami structure, the movement of the origami structure can be controlled, and the results of studies on origami-type actuators have been published [40–43]. In addition, a study was conducted to configure a hydraulic damper by adjusting the size of the outlet of an origami tube that moved in one direction with hydraulic oil [44].

However, there are currently no research results on origami hydraulic dampers that can handle curved strokes and that can be applied to complex excitation conditions, including impact, by taking advantage of an origami structure that can be folded freely.

This study proposes an origami hydraulic damper applicable to a new arc-shaped stroke. The damping effect of the origami hydraulic damper was theoretically analyzed, and a formula for calculating the damping force required for practical use was derived. For verification purposes, a shock vibration system consisting of a mass block, a cantilever elastic leaf spring, and an origami hydraulic damper was devised. The governing equations of nonlinear dynamics were established, and a numerical vibration analysis method was established using the Runge–Kutta method. An origami hydraulic damper experimental unit was fabricated using a thin polypropylene material, and an impact experimental device with an arc-shaped stroke was developed. The numerical analysis value of the actual impact displacement was compared with the measured experimental value, and its accuracy was confirmed. In addition, the impact input energy, diameter of the orifice hole, and type of hydraulic oil were varied, and their effects on the impact damping were examined in detail.

2. Materials and Methods

2.1. Origami-Type Hydraulic Damper. As shown in Figure 1, a cylindrical hydraulic damper, which is installed to reduce the vibration of a vehicle running under complicated road conditions, absorbs the vertical impact load F_z.

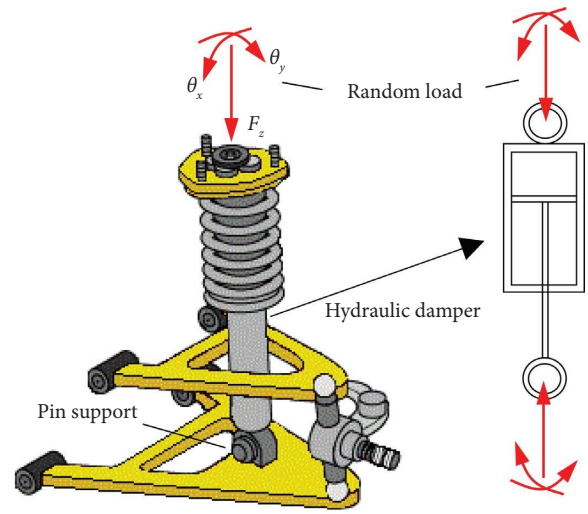

Figure 1: Cylindrical hydraulic damper in a complex vibration environment.

Simultaneously, it absorbs disturbing vibration loads in the longitudinal and lateral directions.

However, when a cylindrical hydraulic damper is used to absorb a complex impact load, as shown in Figure 1, it is supported by a multijoint pin attached to the tip of the load to absorb disturbing vibrations from the lateral direction. Therefore, it is conceivable that the stress concentration occurs around the pin support point. Furthermore, it appears that the wear of the seal of the hydraulic cylinder damper is significantly affected by the disturbing vibration in the lateral direction.

To solve these problems, this study proposes a new origami-type hydraulic damper, as shown in Figure 2, instead of the conventional cylinder-type hydraulic damper, by utilizing the characteristics of the flexible cylindrical origami structure.

As shown in Figure 2, when a complex turbulent vibration load is applied to an origami hydraulic damper, the cylindrical origami structure can flexibly handle the three-dimensional load. Furthermore, an orifice hole was installed at the end of the cylindrical origami structure, and when the oil filled inside passed through the orifice hole as the cylindrical origami structure expanded and contracted, a damping effect similar to that of an origami hydraulic damper was produced. The damping effect of the origami hydraulic damper could be adjusted by changing the size of the orifice holes.

To verify the characteristics of the origami-type hydraulic damper, as shown in Figure 2, a study was conducted using an arc-shaped, stroke-type verification test device, as shown in Figure 3. The verification test equipment consisted of a vibration model consisting of an elastic cantilever with a mass block attached to the tip, tubular origami hydraulic dampers attached to both sides of the lumped mass block, and a fixed frame.

The flat expansion view of the origami structure is shown in Figure 4. The solid line is the outward folding, and the dotted line is the inward folding. In order to meet

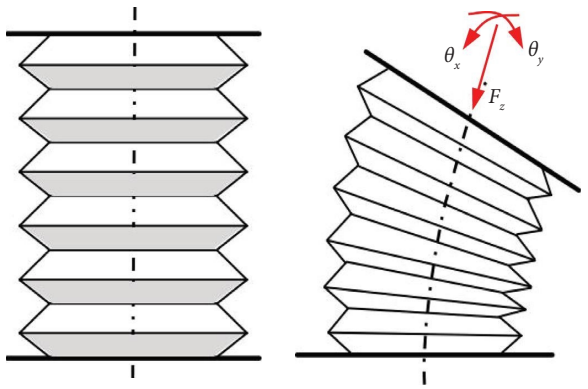

Figure 2: Conceptual diagram of origami hydraulic damper.

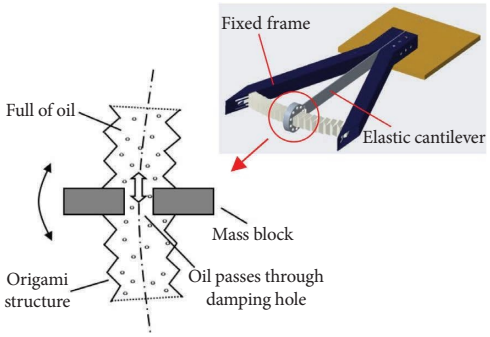

Figure 3: Origami-type hydraulic damper verification test equipment.

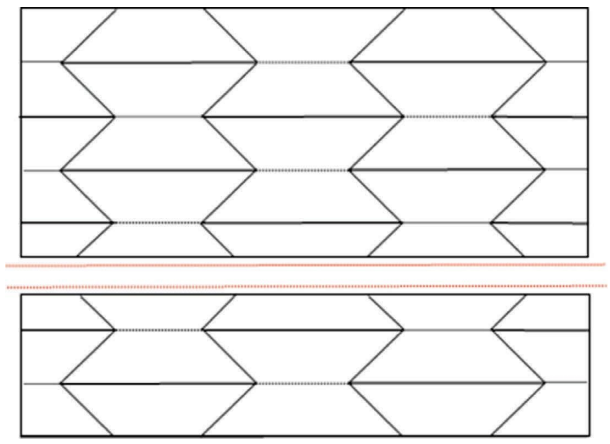

Figure 4: Flat expansion view of origami structure.

the conditions for folding along the axial direction into a cylindrical origami structure with a closed circumference, it is necessary to consider how to identify the inclination angle 1, 2, 3, and 4 of the folded based on the number of segments n of the origami structure, as shown in Figure 5; and the subsequent segments are arranged in an equal isosceles trapezoid array. Since angle 1 is equal to angle 2, 3, and 4, we only need to confirm the size of angle 1 of the fold line is appropriately determined. The conditions for folding are expressed by the following equation:

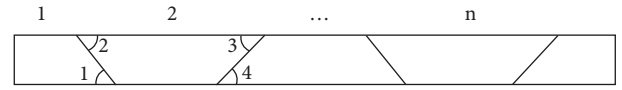

Figure 5: Closing the one unit of cylindrical origami structure.

$$\angle 1 = \angle 2 = \angle 3 = \angle 4 = \frac{\pi}{n}. \tag{1}$$

The folding sequence is shown in Figure 6

An orifice hole was opened at the center of the mass block, and the interior of the cylindrical origami structure was filled with oil. The mass block vibrated by external excitation, and the oil inside flowed between the cylindrical origami structures on both sides through the orifice hole, thereby damping the vibration of the mass block.

2.2. Vibration Characteristic Analysis. To examine the dynamic characteristics of the origami hydraulic damper, the origami hydraulic damper part of the verification test equipment was extracted. Due to the fact that the surface of the origami structure was hardened at the parts of the quadrilateral, as shown in Figure 6, we made rigid assumptions about the surface of the origami structure during simulation analysis, and the origami structure can only move around the creases. The analytical model shown in Figure 7 has been simplified.

In Figure 7, θ is the angular vibration displacement of the mass block, R is the average radius of curvature of the angular vibration trajectory of the mass block, D is the center diameter of the origami hydraulic damper, and d is the diameter of the orifice hole at the center of the mass block. In addition, p_1 and p_2 are the internal pressures of the origami hydraulic dampers on both sides of the mass block, and Q is the flow rate of the fluid inside the origami hydraulic dampers. The flow rate through the orifice hole was calculated as follows [45]:

$$Q = c_f A_1 \sqrt{\frac{2}{\rho}(p_1 - p_2)}, \tag{2}$$

where c_f is the flow coefficient and $c_f = 0.61$. A1 is the cross-sectional area of the orifice hole, and ρ is the density of the oil inside. When a mass block vibrates, the internal flow rate of the origami structure can be calculated using the following equation:

$$Q = A_2 R\dot{\theta}, \tag{3}$$

where A_2 is the average cross-sectional area of the origami structure. $\dot{\theta}$ is the angular vibration velocity of the mass block. Assuming that the flow rate through the origami structure and the orifice hole is the same, we obtain the following equations:

$$A_2 R\dot{\theta} = c_f A_1 \sqrt{\frac{2}{\rho}(p_1 - p_2)}. \tag{4}$$

The average cross-sectional areas of the orifice hole and origami structure are expressed as follows:

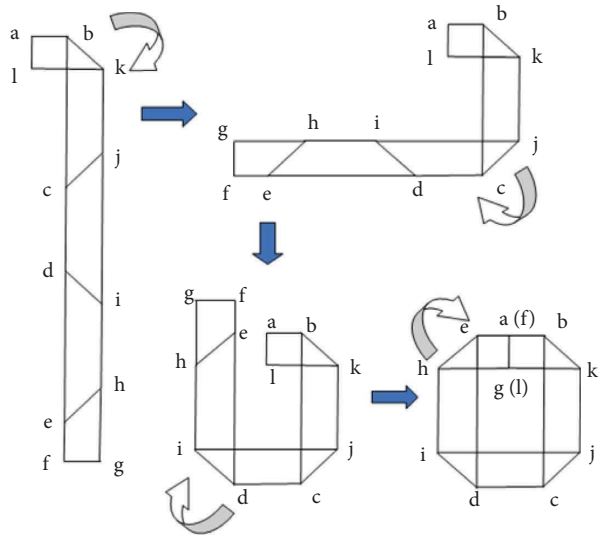

Figure 6: The folding sequence of origami structure.

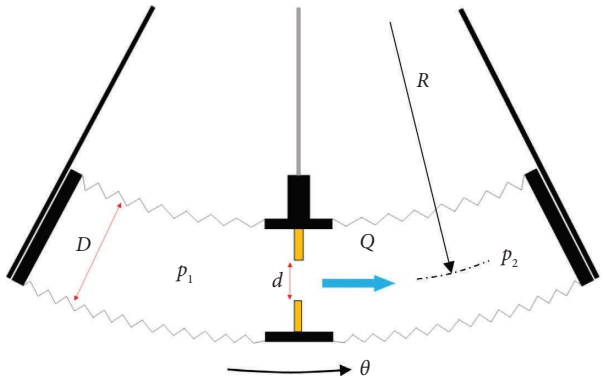

Figure 7: Analysis model of origami-type hydraulic damper.

$$A_1 = \frac{\pi d^2}{4}, \tag{5}$$

$$A_2 = \frac{\pi D^2}{4}. \tag{6}$$

By substituting equations (5) and (6) into equation (4), the following equation is obtained:

$$p_1 - p_2 = \frac{\rho R^2 D^4}{2c_f^2 d^4}\dot{\theta}^2. \tag{7}$$

The damping force acting on the origami hydraulic damper is expressed as follows:

$$F_d = (p_1 - p_2)(A_2 - A_1). \tag{8}$$

By substituting equations (5) and (6) into equation (8), we get

$$F_d = \frac{\pi\rho R^2 D^4\left(D^2 - d^2\right)}{8c_f^2 d^4}\dot{\theta}^2. \tag{9}$$

Equation (9) indicates that the damping force of the origami hydraulic damper has a nonlinear relationship with motion velocity. The coefficient part of equation (9) is defined as the new origami hydraulic damper coefficient, as shown in the following equation:

$$C_d = \frac{\pi\rho R^2 D^4\left(D^2 - d^2\right)}{8c_f^2 d^4}. \tag{10}$$

The damping force of the origami hydraulic damper is expressed by the following equation.

$$F_d = C_d\dot{\theta}^2. \tag{11}$$

The equation of motion for the vibration system considering the damping force of the origami hydraulic damper is expressed as follows:

$$\mathrm{mR}\ddot{\theta} + \mathrm{cR}\dot{\theta} + c_d\dot{\theta}^2 + \mathrm{kR}\theta = -\mathrm{mR}\ddot{\theta}_e, \tag{12}$$

where m is the mass of the mass block, c is the damping coefficient due to friction, k is the stiffness coefficient of the cantilever beam, and $\ddot{\theta}_e$ is the external angular acceleration. Equation (12) shows that the equation of motion of the vibrating system using the origami hydraulic damper includes the squared term of the angular velocity and is a nonlinear differential equation.

For the numerical analysis, the equation of motion (12) was rewritten as the Runge–Kutta standard equation as follows:

$$\frac{\mathrm{d}\dot{\theta}}{\mathrm{d}t} = -\frac{c}{m}\dot{\theta} - \frac{\mathrm{Cd}}{\mathrm{mR}}\dot{\theta}^2 - \frac{k}{m}\theta - \ddot{\theta}_e, \tag{13}$$

$$\dot{\theta} = \frac{\mathrm{d}\theta}{\mathrm{d}t}. \tag{14}$$

If the Runge–Kutta iterative analysis method is applied to equations (13) and (14), the time-series vibration displacement solution as shown in the following equations can be obtained as follows:

$$\theta_0, \theta_1, \theta_2, \theta_3, \cdots, \theta_n. \tag{15}$$

2.3. Verification Experiment Unit. Figure 8 shows the experimental unit of the fabricated origami-type hydraulic damper. As shown in Figure 8, first, we installed a rubber sealing O-ring on the surface of an aluminum cylinder, then nested the metal cylinder at the end of the origami structure, and finally rigidly connected the metal cylinder to the fixed frame. The inside of the origami structure was filled with oil, which was made of thin polypropylene, so that the oil within would not leak. The detailed configuration parameters of the original hydraulic damper experimental unit are listed in Table 1.

As shown in Table 1, the elastic cantilever was made of a SUS304 stainless-steel plate with a length of 500 mm, a width of 50 mm, and a thickness of 2.5 mm. The block mass was 0.617 kg. The average diameter of the origami structure

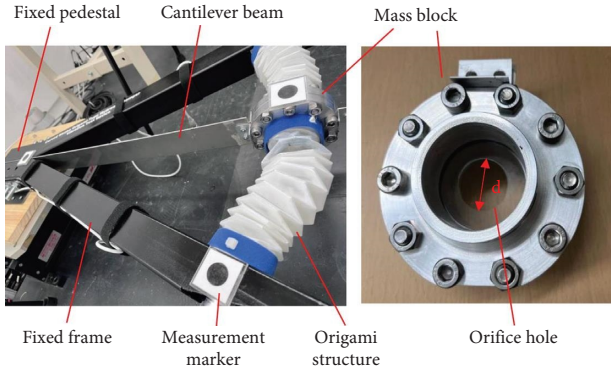

Figure 8: Experimental unit of the origami-type hydraulic damper.

Table 1: Detailed parameters of the experimental unit of the origami hydraulic.

Items	Parameters
Size of cantilever spring (SUS304)	500 mm × 50 mm × 2.5 mm
Mass block weight m	0.617 kg
Average diameter of origami damper D	45 mm
Orifice hole diameter d	40 mm/35 mm/30 mm/ 25 mm

was 45 mm. Four acrylic ring boards with circular holes 40, 35, 30, and 25 mm in diameter were prepared to examine the damping effect of the origami hydraulic damper. The size of the orifice hole of the origami hydraulic damper can be adjusted by fixing the acrylic ring board to the center of the mass block. The moment of inertia of the cantilever beam can be calculated as follows [46]:

$$I = \frac{bh^3}{12} = \frac{0.05 \times 0.0025^3}{12} = 6.51 \times 10^{-11} m^4. \quad (16)$$

The bending stiffness coefficient of the cantilever beam was calculated using the following equation (42):

$$k = \frac{3EI}{L^3} = \frac{3 \times 193 \times 10^9 \times 6.51 \times 10^{-11}}{0.5^3} = 301.54 \frac{N}{m}. \quad (17)$$

By substituting the configuration parameters in Table 1 into equation (9), the relationship between the diameter of the orifice hole and the damping coefficient of the origami hydraulic damper is expressed as shown in Figure 9.

Figure 9 shows that the damping coefficients of the origami hydraulic dampers are 3.88, 1.50, 0.58, and 0.18 when the orifice hole diameters are 25, 30, 35, and 40 mm,

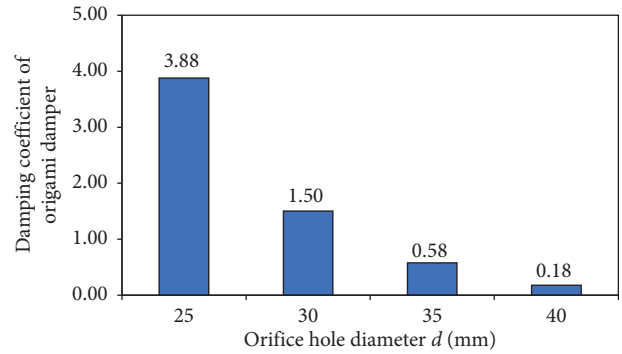

Figure 9: Relationship between diameter of orifice hole and damping coefficient of origami damper.

respectively. This indicates that the orifice hole diameter significantly influences the damping effect of the origami hydraulic damper.

To determine the linear viscous damping coefficient c by friction, the origami structure was removed from the origami hydraulic damper experimental unit, and a basic vibration system consisting of only a mass block and an elastic cantilever was constructed. Subsequently, an initial forced displacement was applied to the basic vibration system, and the response acceleration of the free vibration was measured. The results are presented in Figure 10.

Using the free vibration measurement results shown in Figure 10, damping coefficient c was obtained as follows:

$$c = \frac{\sqrt{mk}}{\pi} \ln\left(\frac{a_1}{a_2}\right) = 0.1 \frac{Ns}{m}, \quad (18)$$

where m is the mass of the mass block, k is the bending stiffness of the cantilever beam calculated using equation (17), and a_1 and a_2 are the adjacent amplitude values, as shown in Figure 10. The results of equation (18) indicate that the frictional linear viscous damping coefficient of the origami hydraulic damper was 0.1 Ns/m.

2.4. Impact Verification Experiment. The impact test apparatus shown to examine the damping effect of the origami hydraulic damper, an impact test apparatus shown in Figure 11 was fabricated. As shown in Figure 11, a steel ball dropped from height h rolls down along the curved rail and impacts the origami hydraulic damper vibration system by colliding with the mass block at the lowest point of the rail.

To measure the motion displacement of the mass block, measurement markers were attached to the fixed frame and mass block, as shown in Figure 11. During the experiment, the motion of the mass block colliding with the steel ball was photographed using a high-speed camera. The obtained moving image data can be read on a personal computer, and tracking software can be used to create the vibration angular displacement data of the mass block. Figure 12 shows a photograph of the developed verification test device.

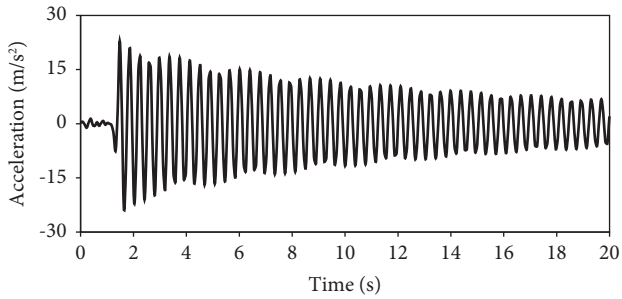

Figure 10: Free vibration result of a system consisting only of a mass block and cantilever.

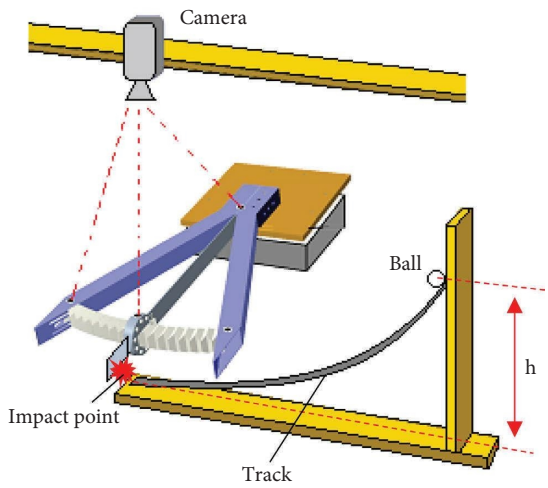

Figure 11: Experimental flow chart of the damping effect measurement of the origami hydraulic damper.

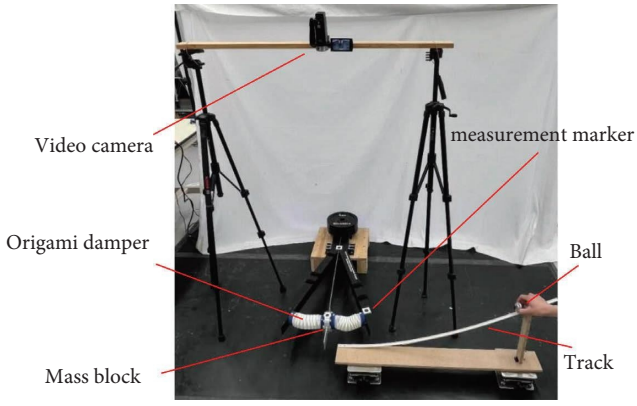

Figure 12: Experiment system to confirm the damping effect of the origami hydraulic damper.

Table 2 lists the configuration parameters of the verification test equipment. The mass of the steel ball used as the impact body was 371 g. To change the magnitude of the impact energy, the heights at which the steel ball started to move were set to 250, 150, and 50 mm.

To confirm the measurement accuracy of the impact test, a measurement test and numerical analysis were performed under the same conditions, and the comparison results are shown in Figure 13.

Figure 13 shows that the trend of change in the measured experimental value and the numerical analysis value match, and the error between the average values of both is 1.57%. However, the peak measurement value of the displacement obtained in the impact experiment was slightly smaller than that in the numerical analysis. This is because the damping coefficient c considered in the analytical model uses a simple approximation. However, in an actual experimental apparatus, the origami structure and friction effect of the internal oil are relatively complicated, and it seems that the approximate value of the analytical model is slightly larger than that of the analytical model.

3. Results and Discussion

To quantitatively evaluate the motion when the mass block was impacted, the standard deviation value calculated by the following formula was used for the motion displacement results obtained in the impact experiment:

$$S = \sqrt{\frac{1}{N}\sum_{i=1}^{N}(\theta_i - \theta_0)^2}, \tag{19}$$

where θ_i is the measured angular displacement value, θ_0 is the average angular displacement value, and N is the number of sample points used in the measurement experiment.

3.1. Effects of Impact Energy. A steel ball with a mass of 371 g was dropped from altitudes of 50, 150, and 250 mm. The angular displacement results for the impacted mass block are shown in Figures 14–16. The solid blue line represents the angular displacement without oil, and the dotted red line represents the angular displacement with oil.

Figures 14–16 show that the angular displacement of the oiled case is obviously smaller than the angular displacement of the nonoiled case. Therefore, it is shown that there is a damping effect due to the damping of the origami hydraulic damper.

Furthermore, to evaluate the damping effect quantitatively, the angular displacement measurement data shown in Figures 14–16 were used to calculate the standard deviation of each angular displacement. The results are presented in Figure 17.

Figure 17 shows that the higher the height at which the steel ball starts to move, the higher the damping effect due to the damping of the origami hydraulic damper. The impact displacement standard deviation decreased by 39.68%, 43.82%, and 47.37% when the starting motion heights of the steel ball were 50, 150, and 250 mm, respectively.

Table 2: Detailed configuration parameters of the verification experiment settings.

Items	Parameters
Mass of steel ball	371 g
Initial height of steel ball motion	250 mm/150 mm/50 mm
Video camera	GZ-E765 (JVC Co. Ltd)
Marker tracking software	MOVIS Neo V3.0 (NAC Image Technology Inc.)

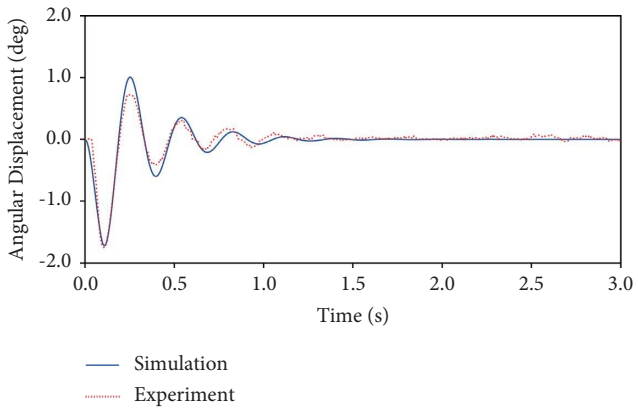

Figure 13: Comparison of experimental and analytical values for impact displacement.

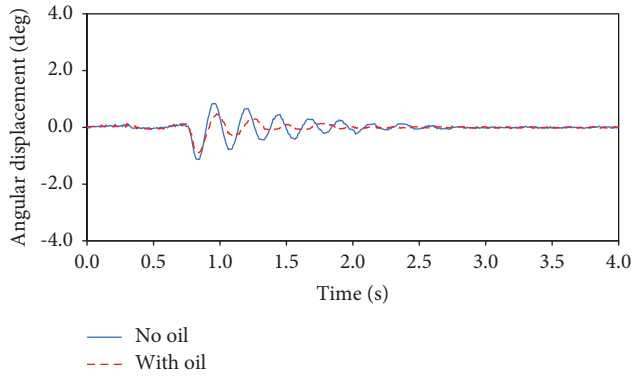

Figure 14: Angular displacement response under the impact of height 50 mm.

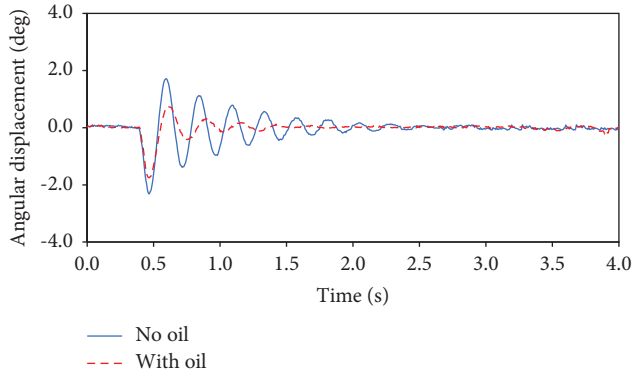

Figure 15: Angular displacement response under the impact of height 150 mm.

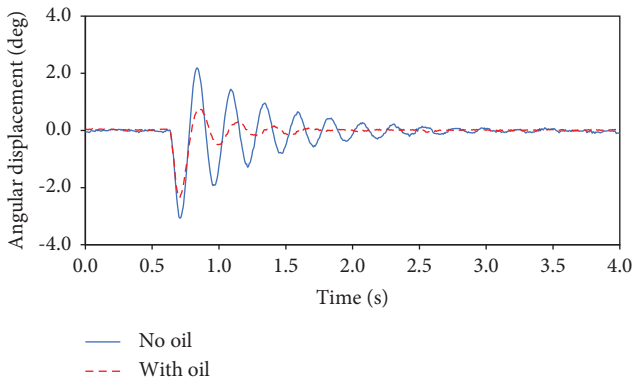

Figure 16: Angular displacement response under the impact of height 250 mm.

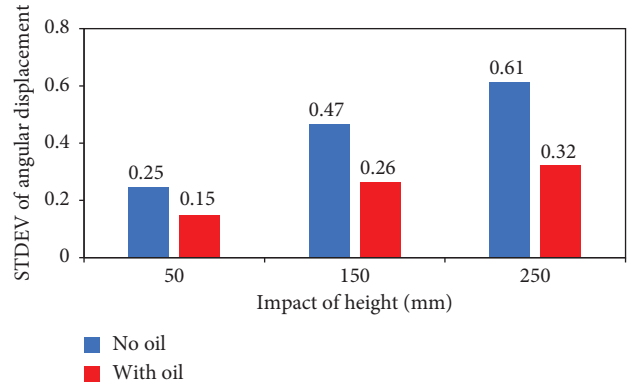

Figure 17: Verification results of damping effect by standard deviation of angular displacement.

Furthermore, to investigate the damping effect in the frequency domain, the displacement measurement data shown in Figures 14–16 were subjected to Fourier transform, and the results are shown in Figures 18–20. The red line shows the results without oil, and the blue line shows the results with oil.

Figures 18–20 show that the main frequency component of the impact load generated in the impact experiment is represented by a frequency of 4.41 Hz, which corresponds to the peak value of the no-oil response graph indicated by the red line. When the origami hydraulic damper is filled with oil, the dominant frequency corresponding to the peak value of the response graph with oil, indicated by the blue line, becomes smaller than that without oil.

The corresponding shock-response peak values for each dominant frequency are listed in Table 3. From the table, it can be confirmed that as the height at which the motion of

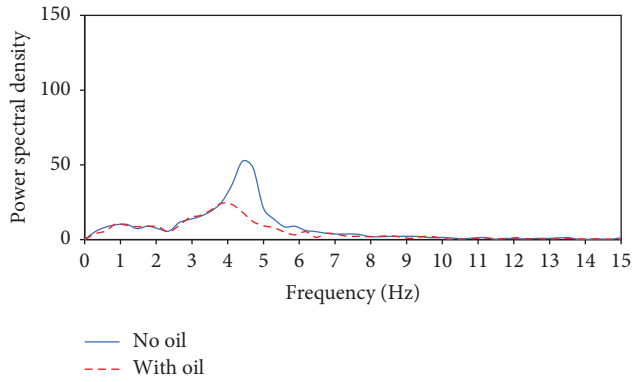

Figure 18: Power spectrum distribution of angular displacement under the impact of height 50 mm.

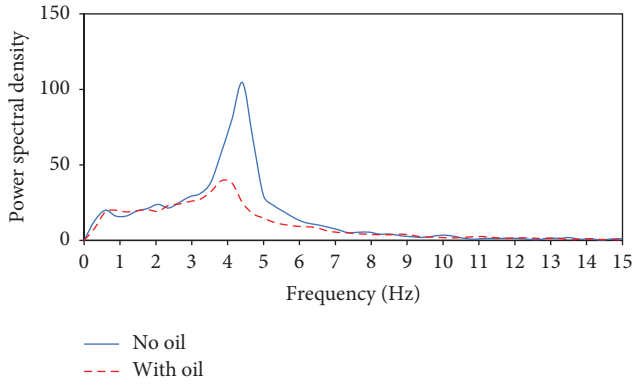

Figure 19: Power spectrum distribution of angular displacement under the impact of height 150 mm.

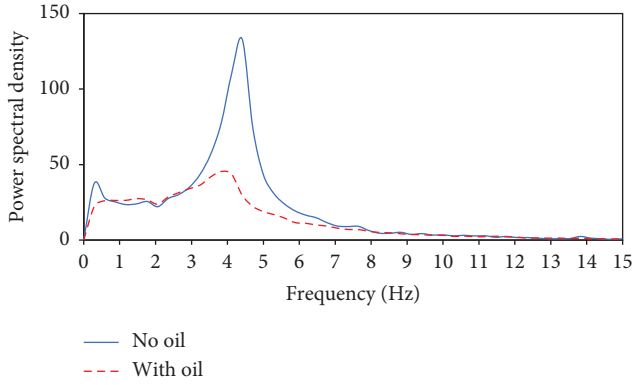

Figure 20: Power spectrum distribution of angular displacement under the impact of height 250 mm.

the steel ball starts increases, the energy input to the impact increases, and the damping effect of the origami hydraulic damper clearly increases. For steel-ball starting motion heights of 50, 150, and 250 mm, the corresponding impact response peak values of the main frequencies were reduced by 53.73%, 62.23%, and 65.86%, respectively.

Table 3: Comparison of response peak values corresponding to the main frequencies.

Impact of height (mm)	No oil	With oil	Damping effect (%)
50	52.43	24.26	−53.73
150	104.52	39.47	−62.23
250	132.98	45.40	−65.86

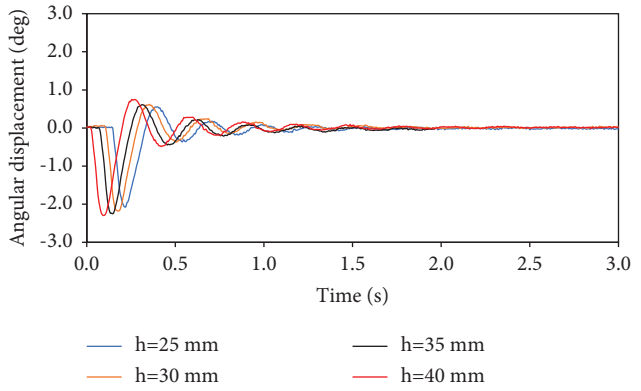

Figure 21: Effect of orifice hole diameter on the damping effect of origami hydraulic damper.

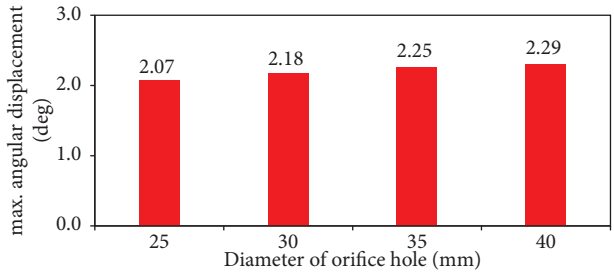

Figure 22: Relationship between orifice hole diameter and maximum angular displacement.

3.2. Effects of Orifice Holes. Figure 21 shows the measurement results of the impact displacement of the mass block when a steel ball with a mass of 371 g was dropped from an altitude of 250 mm, and the orifice hole diameters were 40, 35, 30, and 25 mm. From Figure 21, it can be confirmed that a change in the size of the orifice hole affects the angular displacement.

To quantitatively compare the effects, the maximum impact-angle displacement values corresponding to each orifice-hole test case shown in Figure 21 are summarized in Figure 22. As shown in Figure 22, when the orifice-hole diameters were 25, 30, 35, and 40 mm, the maximum impact-angle displacements were 2.07°, 2.18°, 2.25°, and 2.29°, respectively.

3.3. Effects of Oil Types. For this investigation, the origami hydraulic damper was filled with water and cooking oil, and impact experiments were conducted. The results are

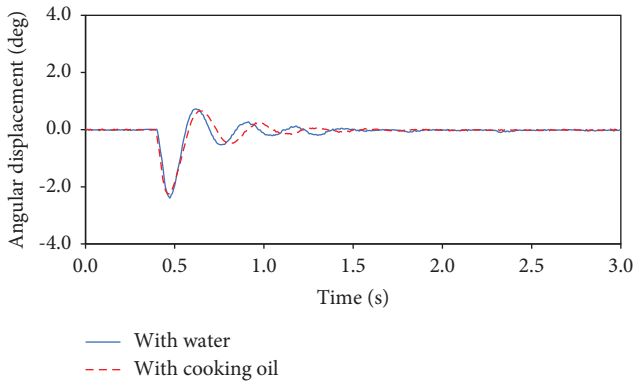

FIGURE 23: Effect of hydraulic oil on the damping effect of the origami hydraulic damper.

presented in Figure 23. The period of damped vibration after impact was relatively longer when cooking oil was used than when water was used. In addition, the maximum angular displacement after impact was 2.39 when using water and 2.25° when using cooking oil, which was 5.86% smaller.

Here, the average viscosity of cooking oil is 0.07 Pas, whereas the viscosity of water is 0.001 Pas. Although the difference in viscosity between the two was approximately 70 times, the difference in the damping effect of the origami hydraulic damper was 5.86%. This indicated that the influence of the hydraulic oil type was relatively small.

4. Conclusions

In this study, an arc-shaped stroke-type origami hydraulic damper was proposed as a new impact energy absorption structure. The following conclusions were drawn from the theoretical examination and verification experiments:

(1) The mechanical characteristics of the proposed arc-shaped stroke-type origami hydraulic damper were investigated, and a formula for the damping force of the origami hydraulic damper was derived. It was proven that the damping force of the origami hydraulic damper was proportional to the square of the angular velocity.

(2) A shock-test device using an arc-shaped stroke-type origami hydraulic damper was developed. A nonlinear motion governing equation including a mass block that absorbs impact energy, a cantilever spring, an origami hydraulic damper, and a damper due to friction was established, and a numerical analysis method using the Runge–Kutta method was proposed. A numerical solution for the impact displacement was obtained, which was consistent with the results of the actual measurement experiment.

(3) Verification experiments were conducted on the impact-vibration damping performance with different impact input energies by varying the motion start height of the steel ball. The impact damping effect strengthened as the impact input energy increased.

(4) Verification experiments were conducted to determine the effect of the orifice hole diameter, which is the main design factor of the origami hydraulic damper, on impact damping performance. The impact damping effect decreased as the orifice hole diameter increased.

(5) To examine the influence of the type of hydraulic oil inside the origami hydraulic damper on the impact damping performance, impact verification experiments were conducted using water and cooking oil. The difference in the impact damping effect was only 5.86% despite the 70 times difference in viscosity between water and cooking oil. Therefore, the type of hydraulic oil had a relatively small effect on the impact damping performance of the origami hydraulic damper.

(6) In the research for this paper, we researched a basic performance of the origami damper, mainly considering the above main effects, and we can ignore other influencing factors due to their smaller impact such as the material of the origami structure, the temperature of the oil, etc. Due to its shape, can adapt to the multidirectional loads, the advantage about the origami damper is that it can be used without any universal joints or other related mechanical structures or in a compact space. Compared with conventional cylinder hydraulic damping devices, they do not require complex mechanical connection structures, which can play a greater advantage in lightweight and compact space. In future work, we will consider the practical applications of the origami dampers problems such as the durability of origami damper and the control of this nonlinear damping characteristic.

Data Availability

The data used to support the findings of this study are available from the corresponding author upon request.

Conflicts of Interest

The authors declare that there are no conflicts of interest regarding the publication of this paper.

References

[1] R. Paswan, J. Das, N. Kumar, A. Kumar, S. K. Mishra, and K. Sujit, "Hydraulic circuit in damper: an overview," *Applied Mechanics and Materials*, vol. 592–594, pp. 2056–2060, 2014.

[2] W. Wang, R. Li, S. Zhu, and Y. Wu, "Effect of mounting and fluid parameters on dynamic damping characteristics of a hydraulic damper," *Vibroengineering Procedia*, vol. 39, pp. 63–68, 2021.

[3] Z. Wu, G. Xu, H. Yang, and M. Li, "Analysis of damping characteristics of a hydraulic shock absorber," *Shock and Vibration*, vol. 2021, Article ID 8883024, 10 pages, 2021.

[4] J. Sun, S. Jiao, X. Huang, and H. Hua, "Investigation into the impact and buffering characteristics of a non-Newtonian fluid

damper: experiment and simulation," *Shock and Vibration*, vol. 2014, Article ID 170464, 10 pages, 2014.

[5] P. Czop, D. Sławik, and G. Wszołek, "Development of an optimization method for minimizing vibrations of a hydraulic damper," *Simulation*, vol. 89, no. 9, pp. 1073–1086, 2013.

[6] H. Gao, M. Chi, L. Dai, J. Yang, and X. Zhou, "Mathematical modelling and computational simulation of the hydraulic damper during the orifice-working stage for railway vehicles," *Mathematical Problems in Engineering*, vol. 2020, Article ID 1830150, 23 pages, 2020.

[7] L. M. Jugulkar, S. Singh, and S. M. Sawant, "Fluid flow modeling and experimental investigation on automobile damper," *Construction and Building Materials*, vol. 121, pp. 760–772, 2016.

[8] M. R. Ahmed, A. R. Yusoff, and F. R. M. Romlay, "Numerical investigation of continuous damping of the SemiActive suspension system for passenger car," *Institute of Physics Conference Series: Materials Science and Engineering*, vol. 530, no. 1, Article ID 12014, 2019.

[9] A. Dobre, "Modelling the dynamic behaviour of car hydraulic dampers," *Institute of Physics Conference Series: Materials Science and Engineering*, vol. 1091, no. 1, Article ID 12018, 2021.

[10] C. S. Dharankar, M. K. Hada, and S. Chandel, "Experimental identification of non-hysteresis algebraic force model of automotive hydraulic damper," *International Journal of Vehicle Performance*, vol. 5, no. 2, pp. 213–231, 2019.

[11] L. Knap, M. Makowski, K. Siczek, P. Kubiak, and A. Mrowicki, "Hydraulic vehicle damper controlled by piezoelectric valve," *Sensors*, vol. 23, no. 4, p. 2007, 2023.

[12] W. Wang, Y. Liang, W. Zhang, and S. Iwnicki, "Effect of the nonlinear displacement-dependent characteristics of a hydraulic damper on high-speed rail pantograph dynamics," *Nonlinear Dynamics*, vol. 95, no. 4, pp. 3439–3464, 2019.

[13] C. Huang and J. Zeng, "Dynamic behaviour of a high-speed train hydraulic yaw damper," *Vehicle System Dynamics*, vol. 56, pp. 1922–1944, 2018.

[14] C. Go, C. Sui, M. Shih, and W. Sung, "A linearization model for the displacement dependent semi-active hydraulic damper," *Journal of Vibration and Control*, vol. 16, no. 14, pp. 2195–2214, 2010.

[15] M. Azimi, A. Rasoulnia, Z. Lin, and H. Pan, "Improved semi active control algorithm for hydraulic damper based braced buildings," *Structural Control and Health Monitoring*, vol. 24, p. 1991, 2017.

[16] M. Shin, C. Lin, and W. Sung, "Numerical analysis for shock absorption performance of accumulated semi-active hydraulic damper," *Journal of Dynamical Systems and Geometric Theories*, vol. 4, no. 1, pp. 29–45, 2013.

[17] K. Hu, F. Li, Z. Zhang, S. Wang, and H. Jiang, "A magnetoelectric hybrid hydraulic damper for the mining robot suspension system," *Shock and Vibration*, vol. 2021, Article ID 5479423, 20 pages, 2021.

[18] J. Gołdasz, B. Sapiński, Ł. Jastrzębski, and M. Kubik, "Dual hysteresis model of MR dampers," *Frontiers in Materials*, vol. 7, p. 236, 2020.

[19] L. B. Raut, Y. M. Khedkar, S. Y. Salunke, and S. V. Jadhav, "Modification of classical hydraulic damper into semi active damper using MR approach," *International Journal of Scientific and Research Publications*, vol. 9, no. 3, pp. 87955–p9683, 2019.

[20] C. Wang, Z. Qiu, Q. Zeng, Y. Liu, and G. Miao, "Energy dissipation mechanism and control model of a digital hydraulic damper," *Shock and Vibration*, vol. 2019, Article ID 1432910, 20 pages, 2019.

[21] S. Vivekananda Sharma and G. Hemalatha, "Numerical and experimental investigation on small scale magnetorheological damper," *International Journal of Engineering*, vol. 35, no. 12, pp. 2395–2402, 2022.

[22] S. V. Sharma and G. Hemalatha, "Small-scale MR damper: design, fabrication and evaluation," *Asian Journal of Civil Engineering*, vol. 24, no. 6, pp. 1489–1499, 2023.

[23] D. Dureisseix, "An overview of mechanisms and patterns with origami," *International Journal of Space Structures*, vol. 27, no. 1, pp. 1–14, 2012.

[24] T. Shen and Y. Nagai, "An overview of folding techniques in architecture design," *World Journal of Engineering and Technology*, vol. 5, no. 3, pp. 12–19, 2017.

[25] A. Lebee, "From folds to structures: a review," *International Journal of Space Structures*, vol. 30, no. 2, pp. 55–74, 2015.

[26] C. Lv, D. Krishnaraju, G. Konjevod, H. Yu, and H. Jiang, "Origami based mechanical metamaterials," *Scientific Reports*, vol. 4, no. 1, p. 5979, 2014.

[27] Y. Hu, Y. Zhou, K. Kwok, and K. Y. Sze, "Simulating flexible origami structures by finite element method," *International Journal of Mechanics and Materials in Design*, vol. 17, no. 4, pp. 801–829, 2021.

[28] Y. Chen, W. Lv, J. Li, and Z. You, "An extended family of rigidly foldable origami tubes," *Journal of Mechanisms and Robotics*, vol. 9, no. 2, Article ID 21002, 2017.

[29] G. Wen, G. Chen, K. Long, X. Wang, J. Liu, and Y. M. Xie, "Stacked-origami mechanical metamaterial with tailored multistage stiffness," *Materials & Design*, vol. 212, Article ID 110203, 2021.

[30] J. Liu, H. Ou, R. Zeng et al., "Fabrication, dynamic properties and multi-objective optimization of a metal origami tube with Miura sheets," *Thin-Walled Structures*, vol. 144, Article ID 106352, 2019.

[31] K. Terada, K. Kadoi, S. Tokura, T. Sushida, and I. Hagiwara, "The deformation mechanism on origami-based foldable structures," *International Journal of Vehicle Performance*, vol. 3, no. 4, pp. 334–346, 2017.

[32] S. Guest and S. Pellegrino, "The folding of triangulated cylinders, Part I: geometric considerations," *Journal of Applied Mechanics*, vol. 61, no. 4, pp. 773–777, 1994.

[33] A. Reid, F. Lechenault, S. Rica, and M. Adda-Bedia, "Geometry and design of origami bellows with tunable response," *Physical Review*, vol. 95, no. 1, Article ID 13002, 2017.

[34] W. Shen, Y. Cao, X. Jiang, Z. Zhang, G. E. Okudan Kremer, and H. Qin, "Experimental and numerical investigation on radial stiffness of origami-inspired tubular structures," *Journal of Applied Mechanics*, vol. 89, no. 3, Article ID 31001, 2022.

[35] X. Wang, H. Qu, and S. Guo, "Tristable property and the high stiffness analysis of Kresling pattern origami," *International Journal of Mechanical Sciences*, vol. 256, Article ID 108515, 2023.

[36] V. Agarwal and K. Wang, "On the nonlinear dynamics of a Kresling-pattern origami under harmonic force excitation," *Extreme Mechanics Letters*, vol. 52, Article ID 101653, 2022.

[37] J. Huang, J. Zhou, Z. Wang et al., "Modular origami soft robot with the perception of interaction force and body configuration," *Advanced Intelligent Systems*, vol. 4, no. 9, Article ID 2200081, 2022.

[38] C. D. Onal, R. J. Wood, and D. Rus, "An origami-inspired approach to worm robots," *IEEE*, vol. 18, no. 2, pp. 430–438, 2013.

[39] S. Wu, Q. Ze, J. Dai, N. Udipi, G. H. Paulino, and R. Zhao, "Stretchable origami robotic arm with omnidirectional bending and twisting," *Proceedings of the National Academy of Sciences of the United States of America*, vol. 118, no. 36, Article ID 2110023118, 2021.

[40] Z. Huang, C. Wei, L. Dong et al., "Fluid-driven hydrogel actuators with an origami structure," *iScience*, vol. 25, no. 7, Article ID 104674, 2022.

[41] S. Ye, P. Zhao, Y. Zhao, F. Kavousi, H. Feng, and G. Hao, "A novel radially closable tubular origami structure (RC-ori) for valves," *Actuators*, vol. 11, no. 9, p. 243, 2022.

[42] J. Liu, Z. Chen, G. Wen et al., "Origami chomper-based flexible gripper with superior gripping performances," *Advanced Intelligent Systems*, vol. 5, no. 10, Article ID 2300238, 2023.

[43] J. He, G. Wen, J. Liu, L. Xue, and Y. M. Xie, "A modular continuous robot constructed by Miura-derived origami tubes," *International Journal of Mechanical Sciences*, Article ID 108690, 2023.

[44] J. Guan, J. Zuo, W. Zhao, N. Gomi, and X. Zhao, "Study on hydraulic dampers using a foldable inverted spiral origami structure," *Vibrations*, vol. 5, no. 4, pp. 711–731, 2022.

[45] Y. A. Cengel and J. M. Cimbala, *Fluid Mechanics: Fundamentals and Applications*, McGraw-Hill, Noida, India, 2006.

[46] F. P. Beer, E. R. Johnston, J. T. Dewolf, and D. F. Mazurek, *Mechanics of Materials*, McGraw-Hill, Noida, India, 2012.